 doi:10.20944/preprints202206.0250.v1

Article

Preparation and Highly Enhanced Eelectrocaloric Effect in a Bimodal-Structured 0.9$KNbO_3$-0.1$BaTiO_3$ Solid Solution at Room Temperature

Hongfang Zhang[1,*], Liqiang Liu[2], Ju Gao[3,1,*], K.W. Kwok[4], Sheng-Guo Lu[5,*], Ling-bing Kong[6], Biaolin Peng[7] and Fang Hou[1]

[1] School of Physical Science and Technology, Suzhou University of Science and Technology, Suzhou, 215009, China
[2] Center for Advanced Ceramics, School of Materials Science and Engineering, Anhui Polytechnic University, Wuhu, 241000, PR. China
[3] School of Optoelectronic Engineering, Zaozhuang University, Zaozhuang, Shandong 277160, China
[4] Department of Applied Physics, The Hong Kong Polytechnic University, Hung Hom Kowloon, Hong Kong
[5] GuangdongProvincial Research Center on Smart Materials and Energy Convesion Devices, Guangdong Provincial Key Laboratory of Functional Soft Condensed Matter, School of Materials and Energy, Guangdong University of Technlogoy, GuangZhou, 51006, China
[6] College of New Materials and New energies, Shenzhen Technology University, Shenzhen 518118, Guangdong, China
[7] School of Advanced Materials and Nanotechnology, Xidian University, Xi'an 710126, China
*Corresponding author: constance_zhanghf@126.com (H.Z.); jugao@hku.hk (J.G.); sglu@gdut.edu.cn (S.L.)

Abstract: The bimodal grain-size distribution 0.9$KNbO_3$-0.1$BaTiO_3$ ceramics, with a typical perovskite structure in tetragonal phase at room temperature, were successfully prepared by an induced abnormal grain growth (IAGG) method at a relatively low sintering temperature. In this bimodal grain-sized distribution structure, the extra-large grains (about 10–50 μm) were evolved from the micron-sized filler powders and the fine grains (about 0.05–0.35 μm) were derived from the sol precursor matrix. The 0.9$KNbO_3$-0.1$BaTiO_3$ ceramics exhibit relaxor-like behavior with the diffused phase transition near room temperature, and confirmed by the existence of the polar nanodomain regions (PNRs) using the HRTEM images. The large room-temperature electrocaloric (EC) effect was found, characterized by an adiabatic temperature drop of 1.5 K, an isothermal entropy change of 2.48 J kg^{-1} K^{-1}, and high EC strengths of $|\Delta T/\Delta E|$ = 1.50×10^{-6} KmV^{-1} and $\Delta S/\Delta E$ = 2.48×10^{-6} J$mkg^{-1}K^{-1}V^{-1}$directly measured under E = 1.0 MV/m. These excellent ECEs demonstrate that this simple IAGG method is highly appreciated for synthesizing high-performance EC materials for efficient cooling devices.

Keywords: electrocaloric effect; abnormal grain growth; bimodal structure; grain-size distribution; polar nanodomain regions

1. Introduction

The electrocaloric (EC) effect refers to the adiabatic temperature change in a polar material under an electric field, due to the isothermal entropy change associated with the electric field induced polarization change [1-3]. The EC effect for a ferroelectric has been attracting continuous attention because of the zero-global-warming-potential applications in solid-state refrigeration, which is regarded as the best solution for cooling microelectronic devices due to the ease of miniaturization, high efficiency, and low cost. Based on these considerations, a "good" EC material should possess the large isothermal entropy change (ΔS) and thus large adiabatic temperature change (ΔT) under a reasonable electric field E. In the other words, large EC strengths defined by $|\Delta T/\Delta E|$ and $\Delta S/\Delta E$ are favored, where parameters T, S, and E are the temperature, isothermal entropy, and applied electric field, respectively. Also, the wide working temperature range near room temperature

Preprints (www.preprints.org) | NOT PEER-REVIEWED | Posted: 17 June 2022 doi:10.20944/preprints202206.0250.v1

(RT) is favored in order to develop high performance EC cooling devices [4-6]. Therefore, one critical question here is how to design and develop high-performance dielectric materials which are capable of generating giant EC effect over a broad T-range near RT, undera relatively low electric field.

A thorough review of the state-of-the-art researches on the EC materials suggests that perovskite relaxor ferroelectrics (RFE) with a similar first-order phase transitions could be suitable solid-state systems because they present the large EC effects with much mild temperature dependency and low hysteresis loss [7, 8]. On the other hand, the quest for an even higher EC effect in bulk ceramic materials is prior to any type of materials other than ceramics, which could be implemented in the medium- and large-scale cooling devices because of the high refrigeration capacity [9]. However, in the recent decades, researchreports on a series of FE perovskite materials in terms of enhanced EC effect revealed that the as-generated ΔT is limited and the largest ΔT is less than 2 K at best in response to $\Delta E < 50$ kV cm^{-1}, a relatively large electric field. This ΔT value could not meet the request of commercial applications [5] and thus substantial effort is still urgently needed.

Additionally, in analogy to the current trends in piezoelectric technology, highly appreciated EC materials should also be lead-free that could in future replace the lead-containing materials for environmental considerations. Among various FE perovskites, $KNbO_3$ (KN)and $BaTiO_3$ (BT), typically environmentally friendly materials of the first-order ferroelectric (FE) transitions, have been paid much attention due to their excellent electrical properties [10]. KN is a well-known FE material that exhibits the same symmetries and phase transition sequence as BT, and it undergoes the structural phase transitions from cubic to tetragonal at its Curie temperature $T = T_c \sim 435^oC$ and further from tetragonal to orthorhombic at ~ 225^{o}C upon cooling from high temperature to room temperature [11]. Although it was theoretically calculated that large EC temperature change can be achieved near the Curie point, e.g. $\Delta T \sim 6$ K at $T \sim 435^oC$ for KN, and $\Delta T \sim 1.5$ K at 12^{o}C for BT [12], these individual materials are not desired for practical cooling device applications due to their best EC performance is achievable only far above RT.

Physically, it is known that appearance of the largest EC effect around T_c for a FE material is ascribed to the fact that external field induced isothermal entropy change usually reaches the largest around T_c. Therefore, a good EC material is required to have its Curie point close to the device operational temperature, such as RT for most practical applications. Furthermore, the thermal hysteresis in terms of FE polarization over the phase transition region should be as weak as possible, since such a hysteresis loop represents the energy loss during the device operation [4]. Keeping in mind these issues, one understands that a good EC system should have its Curie temperature around RT on one hand, and exhibit weak thermal hysteresis on the other hand.

An immediate choice to fit the above requirement is a KN-BT solid solution which allows a remarkable reduction of the Curie point with respect to both KN and BT. And the $0.9KNbO_3$-$0.1BaTiO_3$ (KN-BT(9/1)) solid solution exhibits its Curie temperature of $T_c \sim 50\ ^oC$, which is very close to RT. In addition, a solid solution, consisting of two distinct FE components with remarkably different T_c, favors a diffused phase transition from the high-T paraelectric phase to low-T FE phase, accordingly leading to the weak thermal hysteresis [11].

Nevertheless, so far there has been no report on the EC effect of this KN-BT(9/1) system, mainly because the preparation of highly dense KN-BT(9/1) ceramics has been unsuccessful due to the large differences between the properties of cations involved in KN and BT using the conventional solid-state reaction technology, noting that the melting point of KN is as low as 1040 ^{o}C, but that of BT is as high as 1625 ^{o}C. In addition, the potassium oxide (K_2O) is volatile over 800 ^{o}C and its evaporation from the system can be accelerated by the humidity in the sintering environment, resulting in deviated stoichiometry and thus easy formation of unwanted phases [13]. A proper sintering method to overcome this deficiency would be highly appreciated if one plans to sinter high-quality KN-BT(9/1) ceramics.

Preprints (www.preprints.org) | NOT PEER-REVIEWED | Posted: 17 June 2022 doi:10.20944/preprints202206.0250.v1

In this study, a new sintering technique, the so-called induced abnormal grain growth (IAGG) method developed by us in the previous work [14], was introduced to prepare KN-BT(9/1) ceramics with a novel bimodal grain-size distribution structure via a conventional solid-state reaction simply and easily. This bimodal grain-size microstructure (briefly called the bimodal structure) is consisted of a small amount of large-sized grains uniformly embedded in the matrix of nano & fine-sized grains. And the large grains are evolved from the micron-sized KN-BT(9/1) powders (fillers), simultaneously, the small ones are derived from the nano-sized KN-BT(9/1) particles (matrix), which all are well sintered at a relatively low sintering temperature. Our results reveal that the highly dense and chemically stoichiometric KN-BT(9/1) ceramics can be obtained; also, the excellent EC performance can be exhibited which is capable of generating large EC effect under a small electric field near the RT. These advantages would be characterized by optimizing the processing route and sintering behavior so that the structure– EC property relationship can be developed.

2. Materials and Methods

2.1. Preparation of the filler and matrix powders

Micron-sized KN-BT(9/1) powder (as fillers) was fabricated using KN and BT as raw powder by the conventional ceramic processing. Herein, the KN powder was calcined at 640 °C for 4 h using pure grades of K_2CO_3 and Nb_2O_5 powder as starting materials. Then, the calcined KN was again ball-milled for 24 h and dried at 120 °C for overnight. Subsequently, 0.9 mol KN and commercially high purity nano-sized 0.1 mol BT powder (powder diameter D_{50}=50 nm, SAKAI Chemical Industry Co. Ltd. Japan) were weighed and ball milled, after the drying, the uniformly mixed powder was calcined at 900 °C for 2 h, and then ball-milled for 24 h and dried at 120 °C for overnight for further use, as shown in Fig. S1(a).

A modified Pechini method was introduced to prepare for the KN-BT(9/1) sol precursor. All raw materials were weighed according to the formula. For the Nb-sources, the Nb_2O_5 (99.95%, Alfa Aesar) powder was used and dissolved in hydrofluoric acid (48–51%, ACS, Alfa Aesar) at 80 °C, and then ammonium hydroxide (28% NH_3, Alfa Aesar) was tardily added into the solution until the pH value reached 10, followed by filtering, washing, and drying of the sediment at 80 °C for 10 h. Consequently, the niobium hydroxide was formed. The Nb-source was then obtained by dissolving the niobium hydroxide in citric*acid* (CA) solution. For preparing the metal-CA solution (metal: K and Ba), K_2CO_3 and $BaCO_3$ were dissolved directly in CA solution. For the Ti-CA solution, tetrabutyltitanate ($C_{16}H_{36}O_4Ti$, 96%, Alfa Aesar)with the CA solution was heated to 80 °C until the solution became transparent. Finally, all above metal sources were mixed, and the ratio of CA:EG (ethylene glycol) was set as 1/4 and pH value was set to 10. The KN-BT(9/1) precursor solution was obtained by stirring the solution at 80 °C for 2 h, and dried at 120 °C for 24 h, and then calcined at 900 °C for 2 h as matrix particles. The detailed synthesis routes are shown in Fig. S1(b).

2.2. Preparation of bimodal structure KN-BT(9/1) bulk ceramics

The processing scheme of the IAGG method is shown in Fig. S1(c), firstly, the fillers, i.e., micron-sized KN-BT(9/1) particles was dispersed in nano-sized KN-BT(9/1) powders (as the matrix), and then ball milled for 4 h to form uniform suspension with an assistant of ball media ethanol. The homogeneous slurry was completely dried at 120 °C. Then, the dried powder was used to prepare green pellets with a diameter of 10 mm and a thickness of about 1 mm. Finally, the green pellets were sintered at 1000–1050°C for 2 h in air with a heating rate of 2 °C/min. At the same time, by comparison, the green pellets also were prepared using the conventional ceramic processing, and Sol-gel technique as shown in Figs. S1(a)–(b), and then sintered at 1050 °C for 2 h in air with a heating rate of 2 °C/min respectively.

Preprints (www.preprints.org) | NOT PEER-REVIEWED | Posted: 17 June 2022 doi:10.20944/preprints202206.0250.v1

2.3. Characterizations

2.3.1. Microstructure and morphology

The crystal structures are examined using the X-ray diffraction (XRD, Bruker D8 ADVANCE) with $CuK_{\alpha 1}$ radiation (1.5418 Å, 40 kV, 40 mA) at a scan step of 0.02º at room temperature. The SEM images are applied to observe the natural surface of bulk ceramic samples, also, the composition analysis was done using the energy dispersive X-ray spectroscopy (EDS) with the SEM facility (SEM, JEOL JSM-6335F). A high-resolution transmission electron microscope HRTEM images (Tecnai G2 F20 S-Twin, USA) and the corresponding SAED patterns (Selected Area Electron Diffraction, SAED) were applied to observe the morphologies of micron-sized or nano-sized KN-BT(9/1) powders.

2.3.2. Measurement of the specific heat capacity

The determination of specific heat capacity of the samples was performed using the Mettler Toledo DSC3 instrument according to the Sapphire method. The heat flow was measured directly from -50 – 200 °C, so that the specific heat capacity of the samples can be calculated via:

$$C_{p,sample} = \frac{\Phi_{sam}}{\Phi_{sap}} \frac{m_{sap}}{m_{sam}} C_{p,sap} \quad (1)$$

where $C_{p,sam}$ and $C_{p,sap}$, $\Phi_{p,sam}$ and $\Phi_{p,sap}$, m_{sam} and m_{sap}, are the specific heat (J/K·g), heat flow (W/g), and mass of the sintered KN-BT (9/1) bulk sample at 1050 °C and standard sapphire as reference respectively.

2.3.3. Dielectric and ferroelectric properties

To measure the dielectric and ferroelectric properties, the top and bottom surfaces of the pellet-like samples were coated with Ag paste fired at 600 °C for 30 min as electrodes. The temperature-dependent dielectric spectra were measured over 1 kHz ~ 100 kHz range of frequency using the dielectric analyzer (RT-800, TZDM) from -20 – 500 °C at a rate of 1 K/min. The ferroelectric hysteresis loops were evaluated using a modified Sawyer-Tower circuit operated at a frequency of 10 Hz, over the temperature range from RT to 52 °C.

2.3.4. The setup measurement of electrocaloric effect

The direct ECE measurement was carried out in this study. To directly measure the ECE signals, a pulsed electric field was applied to the sample with a thermocouple (5 precision fine wire thermocouples, Omega Engineering, Inc. USA) attached directly to record the temperature variation as shown in Fig. 1.

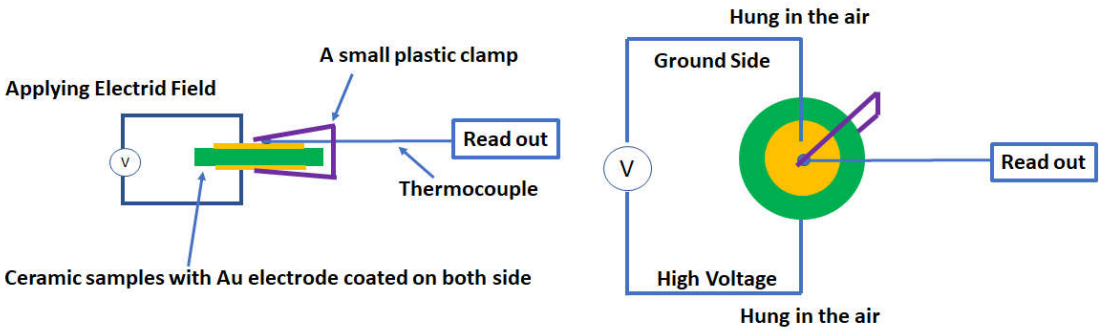

Figure 1. Schematic diagram of the electrocaloric effect measurement setup.

For measurement, the sample was hung in the air through the two wires to avoid any heat dissipations. Thermocouple directly toughed one of the sample surface (ground side) and was connected to an oscilloscope to record the temperature. The measurement was

Preprints (www.preprints.org) | NOT PEER-REVIEWED | Posted: 17 June 2022 doi:10.20944/preprints202206.0250.v1

carried out by (i) manually applying an electric field to the sample witha positive peak appearing on the oscilloscope, (ii) waiting the heat peak to completelypass and temperature curve to become constant, manually removing the electric field, and (iii) appearing a cooling peak. No constant pulse wide of the electric field was set. Based on the dimension of the samples, the period was about 2s. The final cooling performance was obtained by calculating the temperature difference between initial temperature and maximum value of the cooling peak. The precision and validity of thermocouple were checked by 1) a heat plate with known temperature, which was confirmed by another infrared (IR) thermometer, was used to check the precision of the thermocouple, temperature read from thermocouple is in perfect agreement with what read from IR thermometer; 2) before we conducted the ECE measurement on ceramic samples, a Teflon plate with same Au electrode coated on each side was used to check the validity. As shown in the schematic diagram, we use Teflon plate to replace the ceramic samples and applied similar electric field, no temperature changes can be read from thermocouple. Therefore, the observed temperature changes in ceramics samples should be real temperature change.

3. Results and Discussion

3.1. Microstructure of the Bimodal structure

Fig. 2(a) shows the XRD patterns: (1) the commercial nano-sized BT powders; (2) micron-sized KN powders (calcined at 600 °C); (3, 4) micron-sized fillers and nano-sized matrix of KN-BT(9/1) particles calcined at 900 °C, together with (5) the bimodal structure KN-BT(9/1) bulk ceramic sintered at 1050 °C using the IAGG method, and Figs. 2(b)-(c) show TEM images of fillers and matrix of KN-BT(9/1) powders calcined at 900 °C.

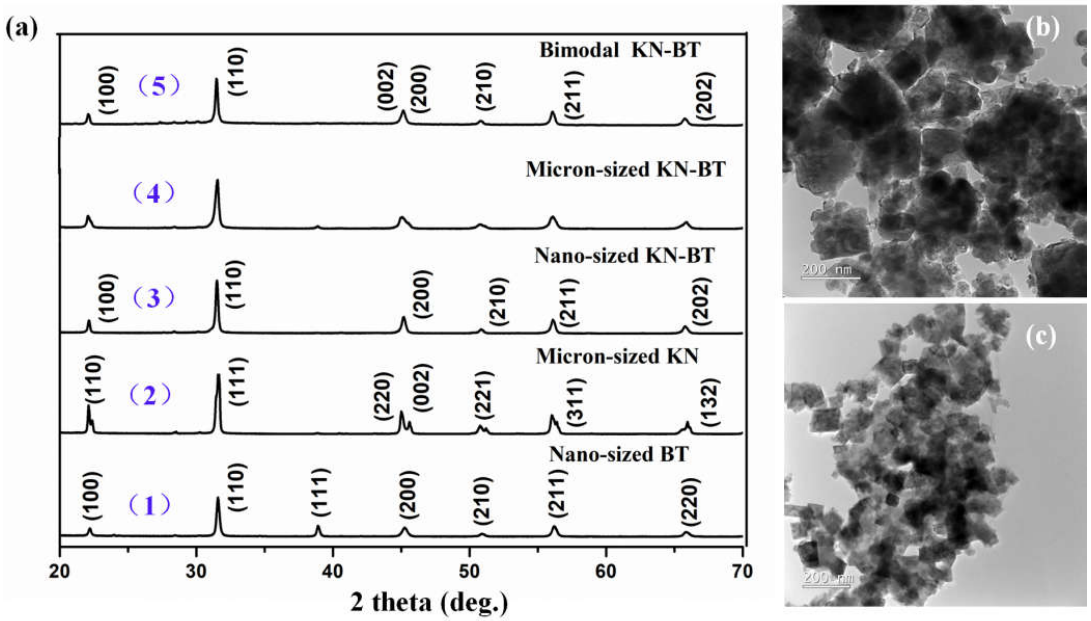

Figure 2. (a) XRD patterns of the powders (1–4), (5) the bimodal structure KN-BT(9/1) bulk ceramics. (b)-(c) TEM images of the micron-sized fillers and nano-sized matrix powders calcined at 900 °C respectively.

As shown in Fig. 2(a), it clearly displays that all the samples exhibit the typical perovskite structures, and the commercial nano-sized BT powder exhibits the cubic perovskite (PDF: 31-174) [15]. As well known, for perovskite compounds, the orthorhombic and tetragonal structures demonstrate different lattice distortions with respect to the cubic structure. And the orthorhombic phase (O-phase) and tetragonal phase (T-phase) can be characterized by checking the reflection splitting. This occurs for the O-phase in the $(220)_O/(002)_O$ reflections, and for the T-phase in the $(200)_T/(002)_T$ peaks respectively. Therefore, in Fig. 2(a), the calcined KN powder exhibits the O-phase due to the $(220)_O/(002)_O$

 doi:10.20944/preprints202206.0250.v1

splitting with higher left peak than the right one (PDF: 32-0822) [16]. And for the bimodal structure sintered KN-BT(9/1) bulk ceramic at 1050 °C, the zoom-in view of 44–47° as shown in Fig. S2, the structure featured with a weak-left and high-right for T-phase structure is demonstrated as T-phase in this study, which is agreement with phase transition diagram in KN-BT system [11].

In Figs. 2(b)–(c), the TEM images reveal micron-sized KN-BT(9/1) powders, as the fillers, consist of the irregular crystalline particles with average grain size of about 200–500 nm, and nano-sized KN-BT(9/1) powders, as the matrix, are characterized as uniform rectangle crystalline particles with grain size about 100 nm respectively.

Also, Fig. S3 shows XRD patterns of the KN-BT (9/1) bulk ceramics prepared by using the conventional ceramic processing, sol-gel technique and IAGG method sintering at 1050 °C respectively. As shown in Fig. S3, all the samples exhibit the pure perovskite structure with the same corresponding peaks.

Fig. 3 shows morphologies of the KN-BT(9/1) bulk ceramics fabricated using the IAGG method sintered at (a) 1000 °C, and (b) 1050 °C, including (e) the cross-section images of samples sintered at 1050 °C respectively. Figs. 3(c) and (d) show the average grain size and size distribution of the bimodal structure of the KN-BT(9/1) bulk ceramics sintered at 1000 and 1050 °C, which were evaluated by using the software equipped with the SEM equipment using a number of both surface and cross-sectional SEM images at different magnifications.

Clearly, the primary character for a bimodal structure is demonstrated by the two well-separated distribution peaks. As shown in Figs. 3(c) and (d), the bimodal grain size distribution suggests that a higher sintering temperature shifts the two peaks simultaneously, a reasonable consequence is due to the faster grain growth at higher sintering temperature. For the 1000 °C sintered sample, only a small number of grains are larger than 1.0 μm in size, surrounded by nano-sized grains of ~ 0.1 μm. When the sintering temperature is increased to 1050 °C, these relatively large grains began to be exaggerated and elongated. Eventually, ultra-large grains with sizes of ~ 10 μm to 50 μm can be found. It can then be concluded that this IAGG method does make sense in accessing the bimodal grain-size distribution with a small number of coarse grains uniformly distributed in fine matrix grains.

Here, an essential issue should be concerned about the composition homogeneity in the coarse and fine grains. To check this issue, the cross-sectional surface image with large amplification as shown in Fig. 3(e), the EDS probed data on the coarse and fine grains respectively are plotted in Fig. 3(f). Indeed, the EDS data indicate that the measured stoichiometry of the large grains is very close to that of the fine-sized grains within the measuring uncertainties. This result is highly concerned and confirms that the IAGG method is powerful for obtaining such bimodal structure with composition homogeneity over the whole samples, in other words, the IAGG method did not trigger the uneven distribution of K^+ and Nb^{5+}in the two types of grains.

Preprints (www.preprints.org) | NOT PEER-REVIEWED | Posted: 17 June 2022 doi:10.20944/preprints202206.0250.v1

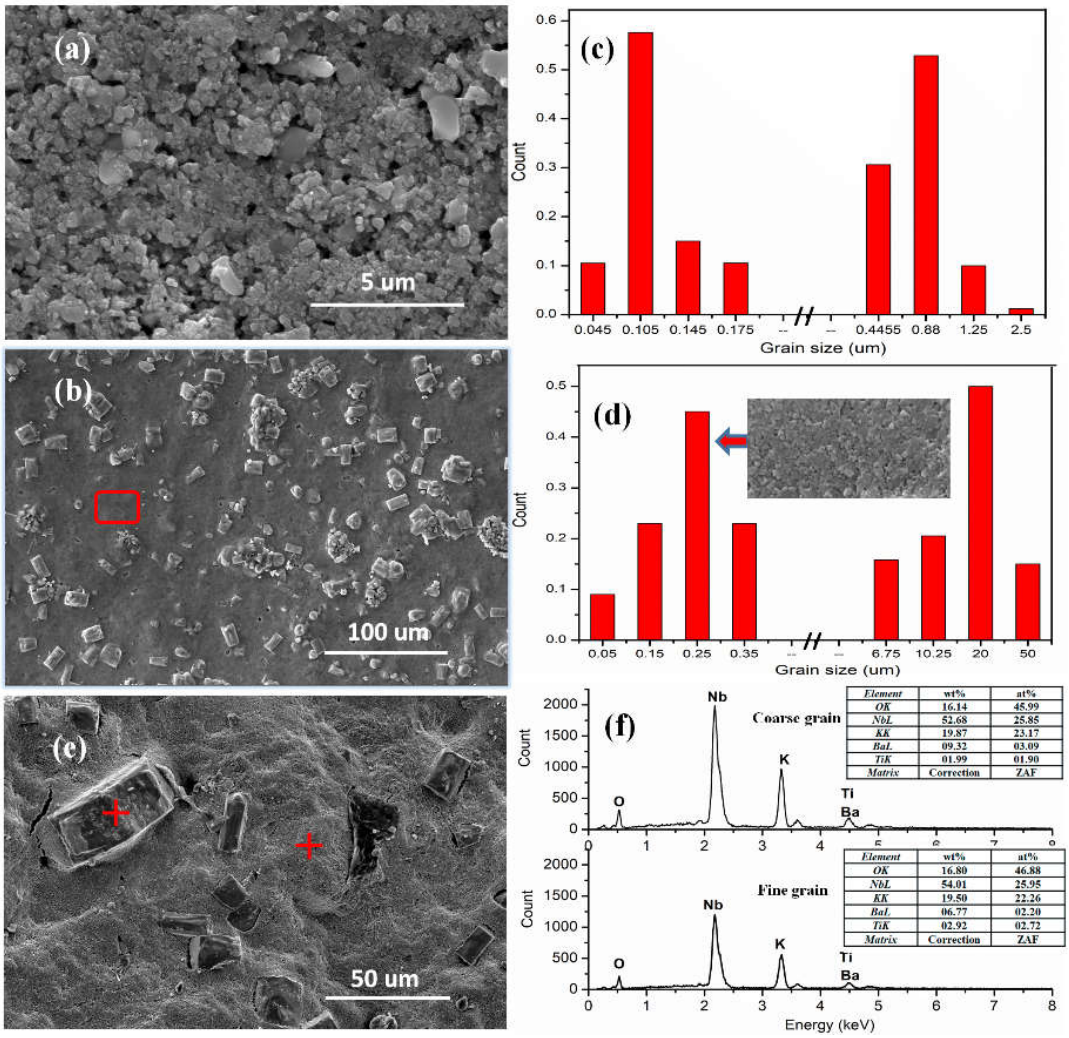

Figure 3. SEM images of the KN-BT(9/1) bulk ceramics sintered at (a) 1000 °C, and (b) 1050 °C, together with their grain sized distributions corresponding to (c) and (d). (e) Cross-sectional SEM image of the KN-BT(9/1) bulk ceramic sintered at 1050 °C, and (f) its corresponding EDS analyses results, with marks indicating the selected coarse and fine grains. The inset of Fig. 3(d) is the enlarged image of matrix marked by the red solid dash square in Fig. 3(b).

Preprints (www.preprints.org) | NOT PEER-REVIEWED | Posted: 17 June 2022 doi:10.20944/preprints202206.0250.v1

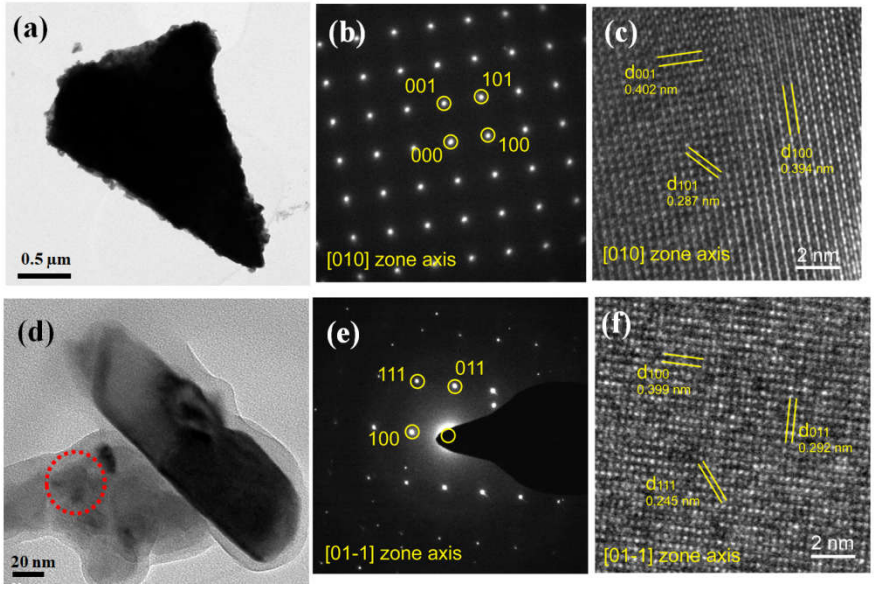

Figure 4. HRTEM images and SAED patterns of (a, b, c) coarse grain, (b, e, f) small grain. The bi-modal structure KN-BT(9/1) bulk ceramic sintered at 1050 °C is chosen and analyzed. .

The HRTEM images and the corresponding SAED patterns of the coarse grain in Figs. 4(a, b, c) and the fine grain in Figs. 4(d, e, f) are indexed respectively in detail. As shown in Figs. 4(b, c), and (e, f), on one hand, the almost identical lattice planes can be found, demonstrating the homogenous structure obtained using the IAGG method; the other hand, the indexed KN-BT(9/1) grains exhibits the characteristic of T-phase structure compared with PDF: 71-0945. Therefore, we can confirm that the present bimodal structure KN-BT(9/1) bulk ceramic is a typical T-phase structure as mentioned above.

Similarly, by comparison, the surface morphologies of the KN-BT(9/1) bulk ceramics fabricated using the conventional ceramic processing and sol-gel technique are shown in Figs. S4(a) and (b), together with (c, d) the corresponding grain size distributions. As expected, these two KN-BT(9/1) bulk samples with unimodal structures and average grain sizes of about 250 nm and 300–400 nm, no abnormal grain growth (AGG) phenomena can be found when sintered at 1050 °C.

The grain growth behavior using the IAGG method can be understood through the explanation of Kingery and Kanget al. [17, 18]. Due to the difference in free-energy across a curved grain boundary, the irregular micron-sized KN-BT(9/1) powder with the large curvature, as the fillers, underwent exaggerated growth, acting as "seed" to consume the neighboring nano-sized matrix. Therefore, in a given polycrystalline system, the grain growth behavior is governed by the maximum driving force(Δg_{max}) relative to the critical driving force (Δg_c), showing the mixed controlling growth behavior. Although the grain size could be increased by sintering at very high temperatures or for very longer times in theory, no grain growth with specific morphologies and crystal orientations of large grains are occurred for aΔg_{max} smaller than aΔg_c. Also, the IAGG method introduced in this study can be used as a reference to develop ceramics with extraordinarily oriented large grains at relatively low sintering temperatures when using the solid-state reaction process. It seems that the filler grains are "cloned", while the gel matrix is just like a "nutrient source or reservoir" to breed the fillers to grow. This method is simple, reproducible and low cost, which can be easily extended many other ferroelectric perovskite-type materials.

3.2. Dielectric and ferroelectric properties

Figs. 5(a)–(b) show dielectric properties of the KN-BT(9/1) bulk sample sintered at 1050 °C: (a) as a function of temperature at 1 kHz, 10 kHz and 100 kHz, and (b) the plot of $\log(\frac{1}{\varepsilon_r}-\frac{1}{\varepsilon_m})$ as a function of $\log(T-T_m)$ at 100 kHz, (c) TEM image of the ferroelectric

Preprints (www.preprints.org) | NOT PEER-REVIEWED | Posted: 17 June 2022 doi:10.20944/preprints202206.0250.v1

nanodomains, (d) the measured specific heat capacity versus temperature. As shown in Fig. 5(a), each of these measured $\varepsilon_r(T)$ curves exhibits a broad peak about 50 °C, indicating a diffused phase transition is present in KN-BT(9/1) bulk ceramic [19], which this diffused behavior is further confirmed by the corresponding dielectric loss curves. Also, it is obvious that the temperature (T_m) of the maximal dielectric constant ($\varepsilon_{r,\max}$) increases with increasing frequency.

For relaxor ferroelectrics, the reciprocal of dielectric constant as a function of temperature follows the Uchino and Nomura function, a modified Curie–Weiss law, which is expressed as [20]:

$$\frac{1}{\varepsilon_r} - \frac{1}{\varepsilon_m} = \frac{(T - T_m)^\gamma}{C} \tag{2}$$

Where C is the Curie constant and γ is the diffusion coefficient ranging from 1 (an ideal normal ferroelectric) to 2 (an ideal relaxor ferroelectric). The slope of the fitting curves is used to determine the γ value in the Fig. 5(b). The value is γ= 1.59 at 100 kHz, confirming the relaxor-like ferroelectric behavior of the KN-BT(9/1) bulk sample.

The ferroelectric nanodomains are observed through HRTEM images as shown in Fig. 5(c), displaying the size of about 2–10 nm existing randomly in the nondomain matrix. The presence of the PNRs provides the strong evidence of the diffusion phase occurred during the phase transition in the KN-BT(9/1) bulk sample.

This relaxor-like behavior of the KN-BT(9/1) bulk sample can be explained as follows: the size of Nb^{5+} ($r_{Nb^{5+}}$ = 0.64 Å) is larger than that of Ti^{4+} ($r_{Ti^{4+}}$ = 0.604 Å) for six-coordination (6-CN). Due to the simultaneous occupation of the 6-CN site by Ti^{4+} and Nb^{5+}, the diffused phase transition can be ascribed to the freezing of the displacive-type phase transition, and thus forming the PNRs [21, 22].

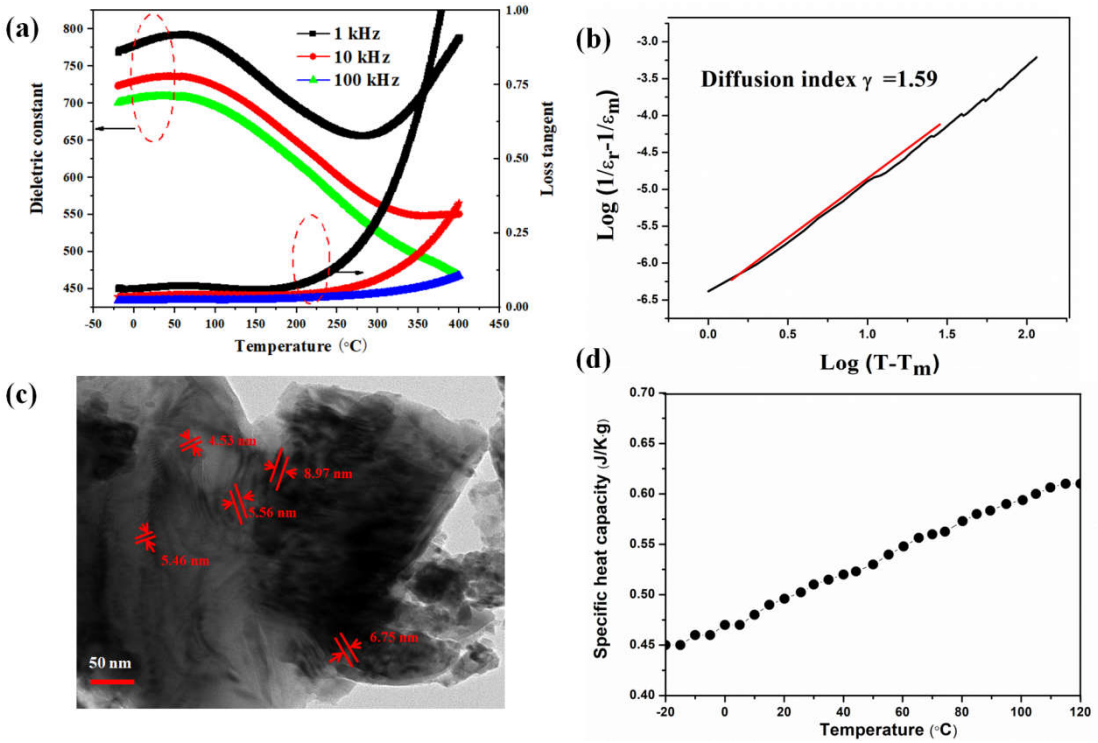

Figure 5. (a) Dielectric properties dependent of the temperature at three selected frequencies (1 kHz, 10 kHz and 100 kHz). (b) The plot of $\log(\frac{1}{\varepsilon_r} - \frac{1}{\varepsilon_m})$ as a function of $\log(T - T_m)$ at 100 kHz. (c) TEM image of polar nanodomain regions (PNRs). (d) The measured specific heat capacity and dielectric properties for the KN-BT(9/1) ceramics.

Moreover, The maximum temperature (T_m) of the bimodal structured KN-BT(9/1)) was observed to be near 50 °C. According to the empirical relation [23]:

Preprints (www.preprints.org) | NOT PEER-REVIEWED | Posted: 17 June 2022 doi:10.20944/preprints202206.0250.v1

$$Tc = \left(\frac{\mathrm{K}}{2\kappa}\right)(\Delta Z^2) \quad (3)$$

where K has the dimensions of a force constant, κ is Boltzmann's constant and Tc is Curie temperature in absolute unit, while ΔZ is the displacement of certain atom. When Ti^{4+} was substituted by Nb^{5+}, the shift (ΔZ) of the tetravalent cation from the octahedron centeris limited, leading to a decrease in T_m. Here, we believed that the presence of the fine-size grains in the bimodal structured sample is responsible for additional decrease in the T_m further [24].

In Fig. 5(d), no obvious anomaly is observed in the specific heat capacity curve, The specific heat capacity value is increased with increasing temperature, which is about 0.50 J K^{-1} g^{-1} at room temperature. As shown in Fig. S5, the enlarged segment of the heat capacity curve can be observed to reveal slightly anomaly. This phenomenon is similar to that of Pb-free relaxor $Ba(Ti_{0.65}Zr_{0.35})O_3$ ceramics [21], when the displacive phase transition is frozen, the specific heat capacity anomaly should be negligibly small (absence of the specific heat capacity anomaly).

Fig. 6(a) shows P-E hysteresis loops of the KN-BT(9/1) bulk sample sintered at 1050 °C measured at RT and 52 °C at 10 Hz, while Fig. 6(b) illustrates the P-E curves at different electrical fields, with the curve of polarization as a function of electric field at RT to be shown as the inset in Fig. 6(b).

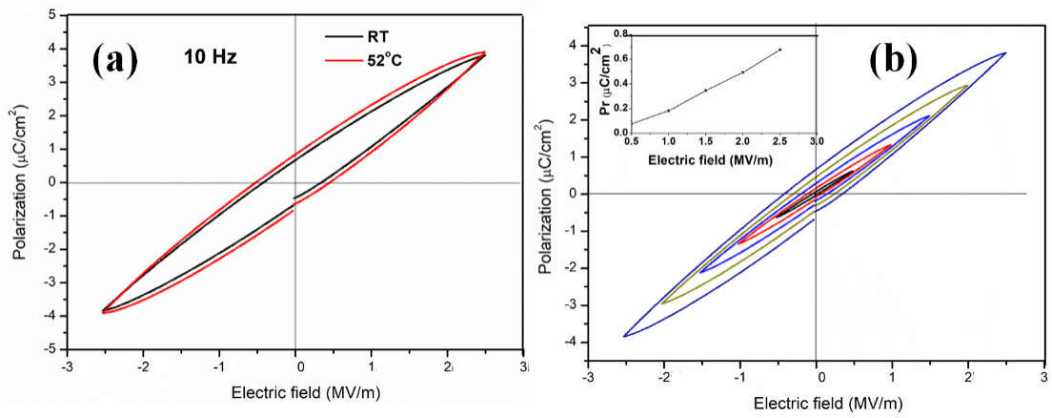

Figure 6. (a) P-E loops measured at RT and 52 °C at 10 Hz. (b) P-E loops measured at different electric fields at RT, with the inset showing the remanent polarization (*P*r) versus electric field.

The sample has ferroelectric nature, whereas the slim P-E hysteresis loops suggest that the diffused phase transition occurred with the low hysteresis losses. The P-E loops at RT and 52 °C were nearly the same, indicating the high performance of ferroelectricity can be reached a relatively broad temperature range at maximum temperature. Also, as seen in Fig. 6(b), the P-E loop is electric field dependent, with the remanent polarization to be increased almost linearly with increasing electric field. At 2.5 MV/m and RT, the values of the *P*r and the coercive field (*E*c) are 0.675 μC/cm² and 0.23 MV/m, respectively. By comparison, the P-E loops of KN-BT(9/1) bulk samples sintered at 1050 °C using the conventional ceramic processing and sol-gel technique are shown in Fig. S6. As shown in Fig. S6, the lossy hysteresis loops are observed, indicating the higher conductive behavior in an unimodal structure compared with the bimodal structure in this KN-BT(9/1) bulk samples. That is, the present bimodal structure bulk ceramic displays the high ferroelectricity with the low dielectric loss, it can be inferred that the extra-large grains ensure a high ferroelectricity, while the fine grains ensure highly relative density suppressing tunneling current occurred in the bimodal structure [25].

Preprints (www.preprints.org) | NOT PEER-REVIEWED | Posted: 17 June 2022 doi:10.20944/preprints202206.0250.v1

3.3. Electrocaloric effect

The ECE adiabatic ΔT refers to the temperature drop induced after removing the electric field, and the ECEs were evaluated at RT. The typical thickness of KN-BT(9/1) bulk sample used in the ECE measurement was 0.264 mm with an *electrode diameter* of 6mm (i.e., area of samples: 28.2743 mm^2). The isothermal entropy change, ΔS, is calculated with $\Delta S = c\,\rho V \Delta T/T$, where c is the specific heat of the ceramic sample, the density ρ is 4.638 g/cm^3, V is the effective volume of the sample. Fig. 7(a) shows the directly recorded ECE signal of the bulk sample at RT under 1 MV/m, where the temperature is demonstrated to rise and drop as the field is applied and removed. The ΔT and ΔS at RT under different electric fields are presented in Fig. 7(b). The ratios of $\left|\Delta T/\Delta E\right|$ and $\Delta S/\Delta E$ (or $\Delta Q/\Delta E$, where $\Delta Q = T\Delta S$) are introduced to express the electrocaloric coefficients (ECE strengths). It is found that the KN-BT(9/1) ceramics have pretty high ECE at $\boldsymbol{E}$ =1 MV/m, corresponding toΔT= −1.5 K, andΔS= 2.48 $Jkg^{-1}K^{-1}$. Accordingly, $\left|\Delta T/\Delta E\right|$ = 1.50*10^{-6} KmV^{-1} and $\Delta S/\Delta E = 2.48\times10^{-6}$ $Jmkg^{-1}K^{-1}V^{-1}$ were obtained at RT. As discussed above, the strongly widened phase transition temperature near RT is responsible for the giant ECE response over a relatively broad temperature range [4, 5].

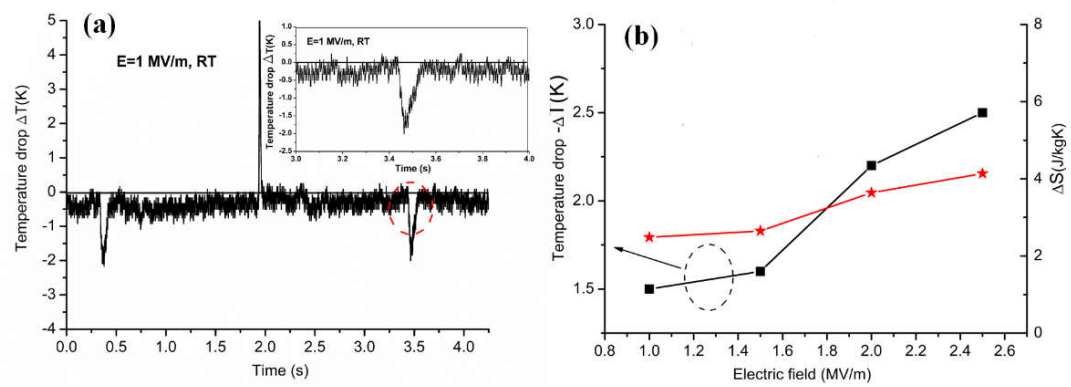

Figure 7. (a) Directly recorded ECE signal for the KN-BT(9/1) sample as the electric field was switched on and off. Solid line is drawn to show the ambient temperature. The magnified temperature drop is shown as the inset, (b) ECE–induced adiabatic temperature drop (ΔT) and isothermal entropy change (ΔS) as a function of electric field ($\boldsymbol{E}$) at RT. The dash line is drawn to guide eyes.

Preprints (www.preprints.org) | NOT PEER-REVIEWED | Posted: 17 June 2022 doi:10.20944/preprints202206.0250.v1

Table 1. Comparison of ECEs for various ferroelectric ceramics with operating temperature near RT.

Material	Form	T (°C)	ΔT (K)	E (MVm^{-1})	$\left\|\Delta T/\Delta E\right\|$ (10^{-6} mV^{-1})	ΔS/ΔE (10^{-6} mkg^{-1}K^{-1}V^{-1})	Method	Reference
KN-BT(9/1)	Ceramic	23	1.5	1	1.50	2.48	Direct	This work
$Ba_{0.65}Sr_{0.35}TiO_3$	Ceramic	23	0.4	2	0.21	–	Indirect	[26]
$Bi_{0.5}Na_{0.5}TiO_3$-based	Ceramic	23	0.45	3	–	–	Direct	[9]
$Ba(ZrxTi_{1-x})O_3$	Ceramic	38	1.1	2.1	0.52	0.54	Direct	[27]
(Pb,La,Ba)(Zr,Sn,Ti)O_3	Ceramic	30	0.25	2.2	0.11	–	Direct	[28]
PZT-5	Ceramic	30	0.15	2.8	0.05	–	Direct	[29]
(Ba,Ca)(Zr,Ti)O_3	Ceramic	60	0.3	2.0	0.15	–	Indirect	[30]
0.9PMN-0.1PT	Ceramic	25	0.63	2.8	0.23	–	Direct	[25]
$BaTiO_3$	Single-crystal	10	1.4	1	1.4	2.3	Direct	[31]
0.9PMN-0.1PT	Single-crystal	50	1.0	4.00	0.25	–	Indirect	[8]

Additionally, as shown in Table 1, compared with the ECEs in ferroelectric ceramics in opening literatures near RT [8-9, 25-31], the current bimodal structure KN-BT(9/1) bulk ceramics in this work shows a fairly high ECE coefficient (strength), which is close to the ECE of single crystal $BaTiO_3$ at 10 °C. Except for the above mentioned a diffused phase transition temperature near RT, on the other hand, the coarse grains (10–50 μm) in the bimodal structure can enhance the dielectric and ferroelectric properties, resulting in high ECE strength at smaller electric fields [24]. At the same time, the finer grains derived from the matrix plays the crucial roles in dense microstructure and inhomogeneous dielectric properties, leading to the high entropy [3].

However, in this study, the unimodal structure KN-BT(9/1) using the conventional ceramic processing and sol-gel technique cannot be evaluated the ECEs due to the occurrence of the strong Joule heating. Apparently, the novel bimodal structure KN-BT(9/1) bulk ceramics can overcome the shortage of the unimodal structure by the IAGG method, also, the preparation of the bimodal structure KN-BT(9/1) ceramics using the IAGG method is highly compatible with the conventional ceramic process, making them potential as micro-refrigerators to be used for cooling the microelectronic devices near RT.

4. Conclusion

The bimodal structure KN-BT(9/1) bulk ceramics in tetragonal phase at RT with a diffused phase transition were prepared successfully using the IAGG method at relatively low sintering temperature of 1050 °C. In this bimodal structure, the exaggerated large grains were evolved from micron-sized KN-BT(9/1) powder (fillers), while the finer grains were derived from the KN-BT(9/1) sol precursor (matrix). Compared with the unimodal structure KN-BT(9/1) bulk ceramics prepared by the conventional ceramic processing and sol-gel technique at 1050 °C, the bimodal structure KN-BT(9/1) bulk ceramics display a high electrocaloric performance with a large ECE-induced adiabatic temperature drop of 1.5 K and a large EC coefficient of $2.48 \cdot 10^{-6}$ Jmkg^{-1}K^{-1}V^{-1} at RT, showing potential for the design of cooling devices. We contribute the coarse grains ensure the high ferroelectricity and ECE strengths, and the finer grains are responsible for the additionally decreased maximum temperature close to the RT, and the inhomogeneity and the increased density. The IAGG method is simple, reproducible and low cost, which can be easily extended to other ferroelectric perovskite-type materials.

Acknowledgments: This work was supported by the National Natural Science Foundation of China (Grant No. 11974304).

References

1. Neese, B.; Chu, B.; Lu, S.G.; Wang, Y.; Furman, E.; Zhang, Q.M. Large electrocaloric effect in ferroelectric polymers near room temperature. *Science* **2008**, *321*, 821–823.
2. Mischenko, A.S.; Zhang, Q.; Scott, J.F.; Whatmore, R.W.; Mathur, N.D. Giant electrocaloric effect in thin-film $PbZr_{0.95}Ti_{0.05}O_3$. *Science* **2006**, *311*, 1270–1271.
3. Qian, X.S.; Han, D.L.; Zheng, L.R.; Chen, J.; Tyagi, M.; Li, Q.; Du, F.H.; Zheng, S.Y.; Huang, X.Y.; Zhang, S.H.; et al. High-entropy polymer produces a giant electrocaloric effect at low fields. *Nature* **2021**, *600*, 664–669.
4. Shi, J.; Han, D.; Li, Z.; Yang, L.; Lu, S.-G.; Zhong, Z.; Chen, J.; Zhang, Q.M.; Qian, X. Electrocaloric cooling materials and devices for zero-global-warming-potential, high-efficiency refrigeration. *Joule* **2019**, *3*, 1200–1225.
5. Barman, A.; Kar-Narayan, S.; Mukherjee, D. Caloric effects in perovskite oxides. *Adv.Mater.Interfaces* **2019**, *6*, 1900291.
6. Gu, H.; Qian, X.; Li, X.; Craven, B.; Zhu, W.; Cheng, A.; Yao, S.C.; Zhang, Q.M. A chip scale electrocaloric effect based cooling device. *Appl. Phys. Lett.* **2013**, *102*, 122904.
7. Tuttle, B.A.; Payne, D.A. The effects of microstructure on the electrocaloric properties of $Pb(Zr,Sn,Ti)O_3$ ceramics. *Ferroelectrics* **2011**, *37*, 603–606.
8. Luo, L.; Chen, H.; Zhu, Y.; Li, W.; Luo, H.; Zhang, Y. Pyroelectric and electrocaloric effect of <111>-oriented 0.9PMN–0.1PT single crystal. *J.Alloy.Compd.* **2011**, *509*, 8149–8152.
9. Li, G.H.; Shi, C.; Zhu, K.; Ge, G.L.; Yan, F.; Lin, J.F.; Shi, Y.J.; Shen, B.; Zhai, J.W. Achieving synergistic electromechanical and electrocaloric responses by local structural evolution in lead-free BNT-based relaxor ferroelectrics. *Chem.Eng.J.* **2022**, *431*, 133386.
10. Lines, M.E.; Glass, A.M. *Principles and applications of ferroelectrics and related materials*. Oxford university press: New York, NY, USA, **1977**; Volume *66*.
11. Bratton, R.J.; Tien, T.Y. Phase transitions in the system $BaTiO_3$-$KNbO_3$. *J.Am.Ceram.Soc.* **1967**, *50*, 90–93.
12. Birks, E.; Dunce, M.; Sternberg, A. High electrocaloric effect in ferroelectrics. *Ferroelectrics* **2010**, *400*, 336–343.
13. Pribosic, I.; Makovec, D.; Drofenik, M. Chemical synthesis of $KNbO_3$ and $KNbO_3$–$BaTiO_3$ ceramics. *J. Eur. Ceram. Soc.* **2005**, *25*, 2713–2717.
14. Zhang, H.F.; Chen, X.; Gao, J.; Lam, K.H.; Liang, S.D.; Fei, L.F.; Mak, C.L.; Chen, J.F. The fabrication and electrocaloric effect of bimodal-grain structure $(Ba_{0.60}Sr_{0.40})TiO_3$ using the induced abnormal grain growth method. *IOP Conf. Ser.: Mater. Sci. Eng.* **2019**, *678*, 012138.
15. Hreniak, D.; Strek, W.; Amami, J.; Guyot, Y.; Boulon, G.; Goutaudier, C.; Pazik, R. The size-effect on luminescence properties of $BaTiO_3$:Eu^{3+} nanocrystallites prepared by the sol–gel method. *J.Alloy.Compd.* **2004**, *380*, 348–351.
16. Kakimoto, K.; Masuda, I.; Ohsato, H. Ferroelectricity and solid-solution
17. structure of $KNbO_3$ ceramics doped with La and Fe. *Key Eng. Mater.* **2004**,
18. 269, 7–10.
19. Kingery, W.D.; Bowen, H.K.; Uhlmann, D.R. *Introduction to ceramics*; John wiley & sons: **1976**; Volume 17.
20. Kang, S.L.; Ko, S.Y.; Moon, S.Y. Mixed control of boundary migration and the principle of microstructural evolution. *J. Ceram. Soc. Jpn.* **2016**, *124*, 259–267.
21. Ravez, J.; Simon, A. Relaxor ferroelectricity in ceramics with composition $Ba_{1-x}Kx(Ti_{1-x}Nb_x)O_3$. *Mater. Lett.* **1998**, *36*, 81–84.
22. Uchino, K.; Nomura, S. Critical exponents of the dielectric constants in diffused-phase-transition crystals. *Ferroelectrics.Lett.* **1982**, *44*, 55–61.
23. Nagasawa, M.; Kawaji, H.; Tojo, T.; Atake, T. Absence of the heat capacity anomaly in the Pb-free relaxor $BaTi_{0.65}Zr_{0.35}O_3$. *Phys. Rev. B* **2006**, *74*, 132101.
24. Abdelkafi, Z.; Abdelmoula, N.; Khemakhem, H.; Simon, A.; Maglione, M. Physical properties of New, Lead Free BaTi1-x(Nb0.5Yb0.5)xO3 Ceramics. *Ferroelectrics* **2008**, *371*, 48–55.
25. Abrahams, S.C.; Kurtz, S.K.; Jamieson, P.B. Atomic displacement relationship to Curie temperature and spontaneous polarization in displacive ferroelectrics. *Phys. Rev.* **1968**, *172*, 551–553.
26. Lu, S.G.; Liu, H.L.; Han, Y.; Zhang, L.Y.; Yao, X. Phase-transition of nanophase ferroelectric $PbTiO_3$ ultrafine powders. *Ferroelectrics.Lett.* **1994**, *18*, 115–120.
27. Vrabelj, M.; Ursic, H.; Kutnjak, Z.; Rozic, B.; Drnovsek, S.; Bencan, A.; Bobnar, V.; Fulanovic, L.; Malic, B. Large electrocaloric effect in grain-size-engineered $0.9Pb(Mg_{1/3}Nb_{2/3})O_3$-$0.1PbTiO_3$. *J. Eur. Ceram. Soc.* **2016**, *36*, 75–80.
28. Bai, Y.; Han, X.; Ding, K.; Qiao, L.J. Combined effects of diffuse phase transition and microstructure on the electrocaloric effect in $Ba_{1-x}Sr_xTiO_3$ ceramics. *Appl. Phys. Lett.* **2013**, *103*, 162902.
29. Qian, X.S.; Ye, H.J.; Zhang, Y.T.; Gu, H.M.; Li, X.Y.; Randall, C.A.; Zhang, Q.M. Giant electrocaloric response over a broad temperature range in modified $BaTiO_3$ ceramics. *Adv. Funct. Mater.* **2014**, *24*, 1300–1305.
30. Wang, J.; Yang, T.; Chen, S.; Li, G.; Yao, X. Characteristics and dielectric properties of $(Pb_{0.97-x}La_{0.02}Ba_x)(Zr_{0.72}Sn_{0.22}Ti_{0.06})O_3$ ceramics. *J.Alloy.Compd.* **2012**, *539*, 280–283.
31. Wang, J.F.; Yang, T.Q.; Wei, K.; Yao, X. Temperature-electric field hysteresis loop of electrocaloric effect in ferroelectricity-direct measurement and analysis of electrocaloric effect. *Appl. Phys. Lett.* **2013**, *102*, 152907.
32. Bai, Y.; Han, X.; Qiao, L.J. Optimized electrocaloric refrigeration capacity in lead-free $(1-x)BaZr_{0.2}Ti_{0.8}O_{3-x}Ba_{0.7}Ca_{0.3}TiO_3$ ceramics. *Appl. Phys. Lett.* **2013**, *102*, 252904.
33. Bai, Y.; Ding, K.; Zheng, G.P.; Shi, S.Q.; Cao, J.L.; Qiao, L.J. The electrocaloric effect around the orthorhombic-tetragonal first-order phase transition in $BaTiO_3$. *AIP Adv.* **2012**, *2*, 022162.